Reference to published article:
Skierszkan, E.K., Robertson, J.M., Lindsay, M.B.J., Stockwell, J.S., Dockrey, J.W., Das, S., Weis, D., Beckie, R.D., Mayer, K.U., (2019). Tracing molybdenum attenuation in mining environments using molybdenum stable isotopes. *Environmental Science and Technology* 53, 5678–5686. https://doi.org/10.1021/acs.est.9b00766

Tracing molybdenum attenuation in mining environments using molybdenum stable isotopes

Elliott K. Skierszkan,[1,2,*] Jared M. Robertson,[3,4] Matthew B. J. Lindsay,[3] Justin S. Stockwell,[2] John W. Dockrey,[2] Soumya Das,[3] Dominique Weis,[1,5] Roger D. Beckie,[1] and K. Ulrich Mayer[1]

[1]Department of Earth, Ocean and Atmospheric Sciences, University of British Columbia, 2020-2207 Main Mall, Vancouver, BC, Canada, V6T 1Z4

[2]Lorax Environmental Services Ltd., 2289 Burrard Street, Vancouver, BC, Canada, V6J 3H9

[3]Department of Geological Sciences, University of Saskatchewan, 114 Science Place, Saskatoon, SK, Canada, S7N 5E2

[4]O'Kane Consultants Inc., 112 Research Drive, Saskatoon, SK, Canada, S7N 3R3

[5]Pacific Centre for Isotopic and Geochemical Research, Department of Earth, Ocean and Atmospheric Sciences, University of British Columbia, 2020-2207 Main Mall, Vancouver, BC, Canada, V6T 1Z4

Corresponding Author

*E-mail: eskiersz@eoas.ubc.ca

Abstract

Molybdenum contamination is a concern in mining regions worldwide. Better understanding of processes controlling Mo mobility in mine wastes is critical for assessing potential impacts and developing water-quality management strategies associated to this element. Here, we used Mo stable isotope ($\delta^{98/95}$Mo) analyses to investigate geochemical controls on Mo mobility within a tailings management facility (TMF) featuring oxic and anoxic environments. These isotopic analyses were integrated with X-ray absorption spectroscopy, X-ray diffraction, Raman spectroscopy, transmission electron microscopy, and aqueous chemical data. Dissolved Mo concentrations were inversely correlated with $\delta^{98/95}$Mo values such that enrichment of heavy Mo isotopes in solution reflected attenuation processes. Inner-sphere complexation of Mo(VI) with ferrihydrite was the primary driver of Mo removal and was accompanied by a circa 1 ‰ isotope fractionation. Limited Mo attenuation and isotope fractionation was observed in Fe(II)- and Mo-rich anoxic TMF seepage, while attenuation and isotope fractionation were greatest during discharge and oxidation of this seepage after discharge into a pond where Fe-(oxyhydr)oxide precipitation promoted Mo sorption. Overall, this study highlights the role of sorption onto Fe-(oxyhydr)oxides in attenuating Mo in oxic environments, a process which can be traced by Mo isotope analyses.

Graphical Abstract

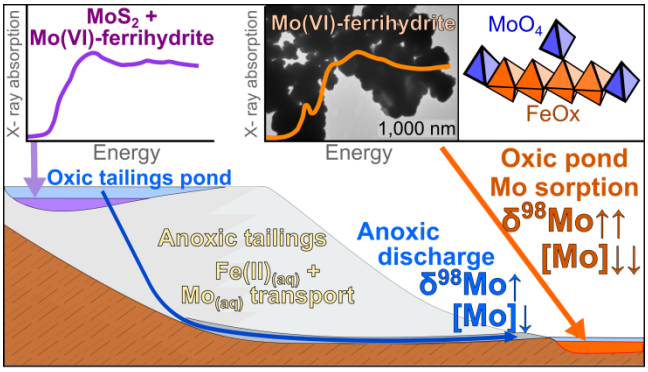

1 Introduction

Oxidative weathering of sulfide mine wastes can release potentially hazardous elements including molybdenum (Mo) to the environment.[1–4] Natural fresh waters typically contain < 1 μg L^{-1} (0.01 mM) of dissolved Mo, whereas mining-impacted waters can exhibit substantially higher concentrations.[3] Excessive Mo exposure can cause biological harm, in particular towards ruminants, which are prone to molybdenosis.[5] The World Health Organization (WHO) health-based maximum concentration is 70 μg L^{-1} (0.73 mM) for drinking water.[6] Although natural waters rarely exceed the WHO criterion,[3] dissolved Mo concentrations exceeding 13,000 μg L^{-1} (137 mM) have been reported in water influenced by mine waste.[7,8] Effective environmental management at mine sites requires a detailed understanding of processes controlling element mobility, but relatively few studies have examined the fate of Mo in mine wastes.[2,8–17]

Molybdenum is released into mine drainage as the molybdate (MoO_4^{2-} oxyanion) through oxidative dissolution of sulfide minerals, where this element may pose an environmental concern. Molybdenite (MoS_2) is the primary source of Mo in most sulfide mineral deposits. Molybdate mobility in the environment is principally controlled by pH-dependent sorption and mineral precipitation-dissolution. Under oxic conditions at pH <6, molybdate is strongly sorbed through inner-sphere complexation with various minerals[18–20] especially Fe-(oxyhydr)oxides.[19–23] This process can attenuate Mo in oxic mine waste-rock.[11] With increasing pH, molybdate sorption involves weaker outer-sphere complexation[19,20,24] which can lead to enhanced Mo mobility in circumneutral to alkaline-pH mine waters.[13] The precipitation of molybdate minerals including powellite [$CaMoO_4$], ferrimolybdite [$Fe_2(MoO_4)_3$], wulfenite [$PbMoO_4$], and nickel(II) molybdate [$NiMoO_4$] constitutes another mechanism of Mo removal in mine wastes.[10,12,13,15–17,25] Under anoxic and sulfidic conditions, Mo attenuation can arise through molybdate conversion to

(oxo)thiomolybdate ($MoO_xS_{4-x}^{2-}$), which precipitates from solution through complexation with Fe(II), S, and organic matter.[26]

Metal stable isotope analyses provide a promising means to trace metal geochemical attenuation.[27–35] Recent studies show that Mo isotopes may be well-suited to this approach.[7,11,36] There are 7 stable isotopes of Mo which undergo isotopic fractionation during sorption and mineral precipitation.[37] Molybdenum isotope fractionation during sorption is caused by molecular distortion of Mo-O bonds[22,38] and preferentially partitions light Mo isotopes into the solid phase.[22,38–40] The same direction in Mo isotope fractionation results from molybdate mineral precipitation under supersaturated conditions, which is thought to be driven by a kinetic isotope effect.[25] Inter-sample Mo isotope variations are expressed by the δ^{98}Mo notation relative to the NIST-SRM-3134 standard, which has a value of +0.25 ‰:[41]

$$\delta^{98}Mo(‰) = \left(\frac{\left(\frac{^{98}Mo}{^{95}Mo}\right)_{sample}}{\left(\frac{^{98}Mo}{^{95}Mo}\right)_{NIST\text{-}SRM\text{-}3134}} - 1 \right) \times 1000 \quad (1)$$

Although Mo stable isotopes can offer insight into Mo attenuation, field application of this technique in mining environments has thus far been limited to two studies of Mo in mine waste rock,[7,11] and none in mine tailings. Mine tailings drainage is often anoxic because tailings are composed of fine-grained material that promotes pore water saturation.[42] Anoxia may enhance the mobility of Mo because Fe-(oxyhydr)oxides,[43] which are important adsorptive surfaces in mine wastes, undergo reductive dissolution or phase transformation which decreases their sorption efficacy.[44] In contrast, waste-rock grain size is coarser and therefore less prone to water saturation and more easily oxygenated, leading to preservation of Fe-(oxyhydr)oxides.[42,45]

The primary objective of this study is to integrate Mo isotope analyses with complementary geochemical and mineralogical techniques to investigate the processes and extent of Mo attenuation in mine wastes. To this effect, a Mo-rich tailings management facility (TMF) that provided opportunities for sampling water and solids along a flowpath featuring oxic and anoxic environments was selected for study. Contrasting redox environments and elevated Mo concentrations provide a suitable setting for investigating Mo attenuation under different geochemical conditions relevant to mine waste and other environments.

2 Materials and Methods

2.1 Study Site

Water and solid-phase samples were collected from the full-scale TMF at a Mo mine in Idaho, USA [the Thompson Creek Mine (TCM), Figure S1]. This TMF holds mine tailings produced between 1982 and 2014 that are composed of various aluminosilicate minerals with a lesser content of molybdenite, pyrite, calcite, and other sulfides. Residual water from the molybdenite extraction process is held in a tailings pond and provides a Mo-rich seepage (mean concentration of ~ 14 µM, Figure S2) to the facility. This seepage percolates to the base of the TMF into a basal drain called the "Rock Toe" (Figure S3). Below the Rock Toe, water flows into a collection pond called the Seepage Return Dam (SRD). Hydrology of the TMF is dominated by infiltration of water through tailings slimes deposited at the bottom of the tailings pond, with a smaller amount of drainage coming from flow through water-unsaturated tailings sands that make up the facility's embankment. A minor component (5 %) of groundwater discharge is also present.[46]

Environmental monitoring of the TMF indicates considerable redox evolution of water between the tailings pond and the Rock Toe, and also between the Rock Toe and the SRD (Figure S3). Surface water in the tailings pond is oxic, but oxidation of residual sulfide minerals and organic chemicals used in mineral processing leads to iron and sulfate-reducing conditions in porewaters within the tailings pond slimes.[46] Porewater pH of the TMF is generally circumneutral, except for localized acidic zones near its base where pyrite-rich tailings were deposited during early construction phases.[46] Basal seepage at the Rock Toe is anoxic as indicated by elevated dissolved Fe, and Mn, but has minimal dissolved sulfide.[46] Upon discharge of Rock Toe seepage into the SRD, oxidation of dissolved Fe(II) drives widespread precipitation of ochreous sludge (Figure S4).

2.2 Water and solid-phase sampling

Water samples were collected to observe the evolution of dissolved Mo under different redox conditions along the TMF flowpath. Sampling locations included the tailings pond, the Rock Toe, and the SRD pond (Figure S1). Water samples in the tailings pond and SRD pond were collected approximately 10 cm below the pond surface. Sampling coincided with either baseflow (October 2014 and October 2015) or freshet (April 2016). All water samples were passed through 0.45 μm filters immediately after collection and refrigerated until laboratory analyses. Appropriate water-sample preservatives were also added in the field: environmental-grade HNO_3 that was further purified by sub-boiling distillation was used to preserve samples for trace element and Mo isotope analyses, and zinc acetate with NaOH was used to preserve samples for dissolved sulfide analyses. Gran titrations were performed in the field to quantify dissolved alkalinity.[47] Water pH was also measured in the field using a MP-20 multi-probe instrument (QED Environmental Systems, MI,

USA) that was calibrated daily using pH 4 and pH 7 buffers. Further sampling method details are described in Skierszkan et al.[11] and in Supporting Information (S.I).

The mineralogical association of Mo was also assessed with solid-phase sampling and analysis. All solid samples were frozen immediately in the field using dry ice and were stored at –20°C until laboratory processing to minimize transformations. Samples of the ochreous precipitates in the SRD pond were collected by various means, including grab-sampling (samples SRD-S1, SRD-S2, and SRD-S4), and vacuum filtering of suspended sediments at the inflow of the SRD (sample SRD-W1 PPTS, isolated on a 0.45 µM filter) (Figure S4). In addition, samples B-1A and Mn-BUCK were obtained by collecting 20 L of Fe(II)-rich seepage at the Rock Toe, allowing it to oxidize over a 6 week period, and isolating the ensuing ochreous precipitates (S.I and Figure S11). Grab samples of tailings slimes (FT-15, FT-16, TC-16, DFT-16) were collected from the bottom of the tailings pond and a grab sample of tailings sand was also collected from the crest of the tailings dam.

Frozen tailings and ochreous precipitate samples were thawed in the laboratory for separation by centrifugation. The supernatant porewaters were discarded, after which the precipitates were rinsed once in ultrapure H_2O (>18.2 mΩ) and centrifuged again. The supernatant solution was discarded and the samples were again frozen and then freeze-dried. For mass spectrometric analyses, precipitate subsamples were dissolved in a HCl-HF-HNO_3 mixture using a microwave digester (MARS6 OneTouch, CEM Corporation) and a five times scale-up of the protocol of ref.[48] Digestion of tailings sub-samples was conducted on a hotplate with successive mixtures of HF-HNO_3, HNO_3, HNO_3-H_3BO_3, and HCl as described in ref.[49]

2.3 Analytical methods

Elemental compositions of waters and digested solids were determined by inductively coupled plasma-mass spectrometry (ICP-MS, Agilent 7700x) and ICP optical-emission spectroscopy (ICP-OES, Varian 725-ES) (S.I). Dissolved anions and sulfide were measured by ion chromatography and colorimetry, respectively (S.I). The average absolute charge balance error in water samples was 3 %, and blanks were monitored to ensure negligible Mo contamination during sampling. The reproducibility and accuracy of ICP-OES and ICP-MS analyses was better than 6 %.[11]

Molybdenum stable isotope ratios of water and digested solid samples were measured by multi-collector ICP-MS (MC-ICP-MS; Nu21, Nu Instruments Ltd.) at the Pacific Centre for Isotopic and Geochemical Research, University of British Columbia, Canada after Mo purification through anion-exchange chromatography and using a ^{97}Mo-^{100}Mo double-spike for instrumental and laboratory fractionation correction.[50] MC-ICP-MS accuracy was verified by processing geological reference materials with well-known δ^{98}Mo values (e.g., USGS BCR-2, SDO-1, Nod-P-1, or seawater; Table S4) with sample batch. Replicate sample δ^{98}Mo analyses showed a precision of 0.1 ‰ or better (Table S1).

The mineralogy of ochreous precipitates was investigated using X-ray diffraction (XRD), Raman spectroscopy, and transmission-electron microscopy (TEM) (S.I). In addition, the local coordination environment and oxidation state of Mo was determined by X-ray absorption spectroscopy (XAS) at the Canadian Light Source HXMA beamline in Saskatoon, Canada. Spectra were obtained over the X-ray absorption fine structure (EXAFS) and X-ray absorption near-edge spectra (XANES) regions. Further details on XAS beamline operation are presented in S.I.

3 Results and Discussion

3.1 Rising δ^{98}Mo indicates attenuation along the flowpath

Water entering the TMF as seepage through the tailings pond begins with a relatively elevated Mo concentration of 34 µM and an isotopic composition of 0.6 ‰. This concentration and δ^{98}Mo reflect dissolution of molybdenite during ore processing. Negligible Mo isotope fractionation is expected in the absence of secondary sorption and precipitation reactions.[11,51–55] As water flows through the tailings facility to its basal discharge point at the Rock Toe and then into the SRD pond, there is a trend of decreasing Mo concentrations and increasing δ^{98}Mo (Figure 1). Basal seepage at the Rock Toe has Mo concentrations $\leq$ 8.4 µM, corresponding to a 75 % decrease relative to the tailings pond. Because groundwater discharge provides < 5 % of the water inputs to the TMF,[46] dilution of tailings seepage cannot account for the decrease in Mo concentrations along the flowpath. In addition, Rock Toe seepage has a δ^{98}Mo of 1.0 ± 0.1 ‰, which is 0.4 ‰ higher than that of the tailings pond. Following discharge of Rock Toe seepage into the SRD pond, δ^{98}Mo values reach a maximum of 2.6 ‰ which coincides with the lowest Mo concentrations (minimum: 0.47 µM) along the flowpath (Figure 1).

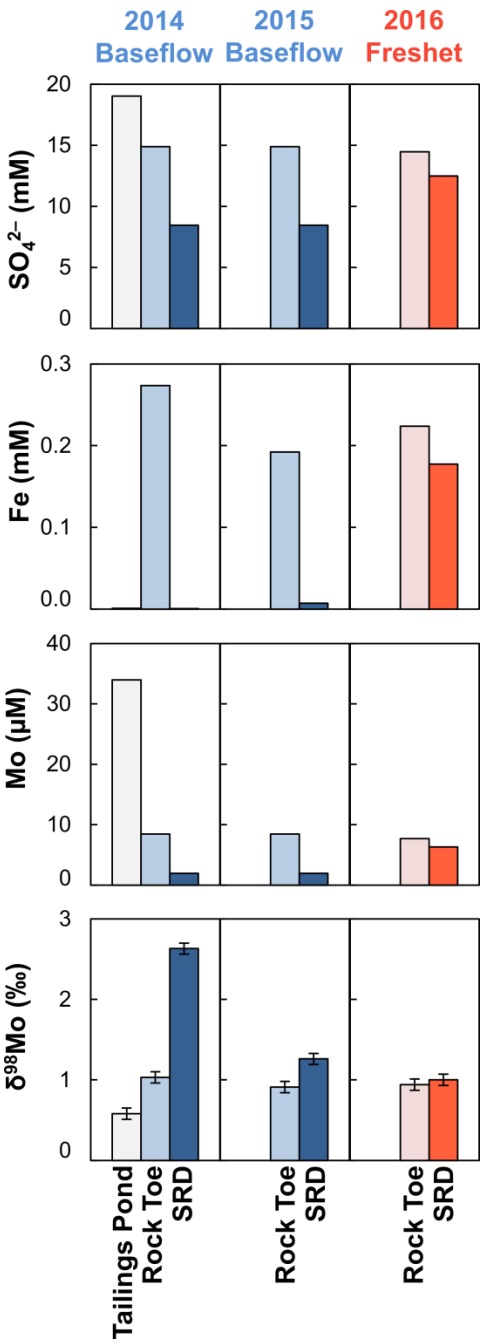

Figure 1. Dissolved SO_4^{2-}, Fe, Mo and δ^{98}Mo in tailings pond, basal tailings drainage at the Rock Toe, and in the SRD pond. Blue colors indicate baseflow hydrological conditions; red colors indicate freshet. Progressive loss of Mo corresponds to a rise in δ^{98}Mo along the flowpath. Between the Rock Toe and the SRD pond, oxidation of dissolved Fe(II) leads to precipitation of Fe-(oxyhydr)oxide minerals and loss of Fe^{2+}, sorption of Mo, and a rise in δ^{98}Mo.

Rising δ^{98}Mo in tailings seepage and decreasing Mo/Cl ratios directly indicate Mo attenuation along the flowpath (Figure 2). All sorption and mineral precipitation reactions for which Mo isotope fractionation factors are known preferentially remove light Mo isotopes from solution.[11,21,22,25,37,56–58] Dissolved Cl concentrations in the tailings pond are orders of magnitude higher than natural groundwater around the TCM and this solute is conservative, making decreasing Mo/Cl another tracer of Mo attenuation that accounts for dilution effects. δ^{98}Mo and Mo/Cl data follow a Rayleigh fractionation pattern[59,60] which is further discussed in section 3.2.

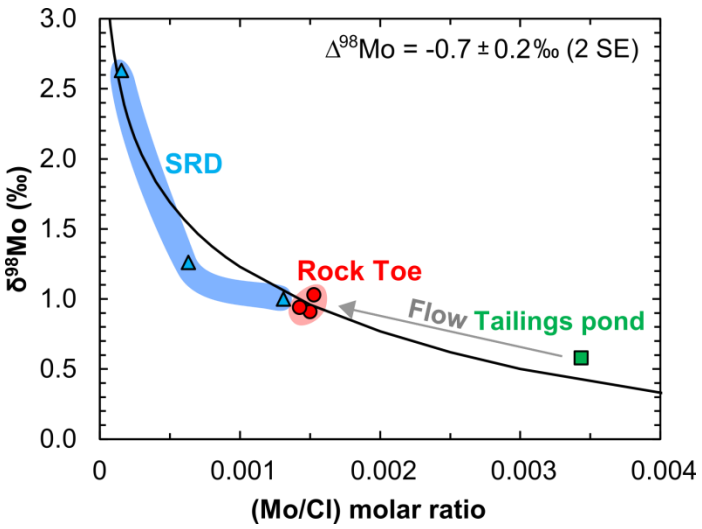

Figure 2. Dissolved Mo attenuation along the flowpath between the tailings pond and the Rock Toe and SRD is demonstrated by rising δ^{98}Mo and a decrease in the ratio of Mo to the conservative solute Cl^-. The black line corresponds to an apparent isotope separation factor (Δ^{98}Mo) of 0.7 ± 0.2 ‰ as determined from a linearized Rayleigh model[59] (Figure S12).

The primary attenuation mechanism that we observed in the TMF is Mo sorption onto Fe-(oxyhydr)oxides, although solid-phase samples were limited to oxic environments within the facility. In the shallow tailings pond sediments, Fe-(oxyhydr)oxides form through pyrite oxidation. Molybdenum speciation in tailings pond samples comprises a mixture of molybdenite and Mo(VI)

sorbed through inner-sphere complexation onto ferrihydrite as determined by linear-combination fitting of the XANES (XANES-LCF) (Figures 3 and S5). These samples have an average δ^{98}Mo of 0.2 ± 0.2 ‰, which is lower than tailings pond water (0.6 ‰) and is also below the average value estimated for molybdenite at the TCM (0.7 ‰).[11] This offset in δ^{98}Mo reflects their composition which is a mixture of molybdenite and isotopically light Mo sorbed to ferrihydrite. Localized low-pH zones that enhance Mo sorption are also found in the water-unsaturated embankment tailings sands where pyrite-rich material was deposited and exposed to oxygen (Figure S6).[46]

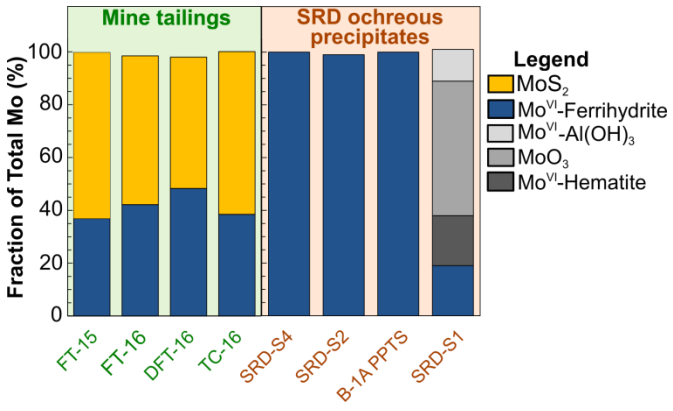

Figure 3. Distribution of Mo in tailings sediments from the tailings pond (left panel with green background) and ochreous precipitates from the SRD pond (right panel with orange background) as determined by linear-combination fitting of X-ray absorption near-edge spectra.

In the SRD pond, downgradient of the TMF, widespread Fe-(oxyhydr)oxide precipitation also occurs through discharge of Fe(II)-rich basal tailings seepage (Figure S4). This process drives Mo sorption and isotope fractionation in the SRD pond, resulting in a substantial decrease in Mo and Fe concentrations and a δ^{98}Mo increase by up to 1.6 ‰ relative to input values (*i.e.*, the Rock Toe) (Figure 1 and Table S3). The decrease in dissolved Mo and Fe concentrations was consistent during the three sampling events, although it was subdued under freshet conditions (April 2016)—possibly because higher flushing rates decreased the residence time of Mo in the SRD pond and

therefore made its aqueous chemistry more reflective of that of the Rock Toe (Figure 1). Ochreous precipitates forming in the SRD pond are characterized by high Mo content, ranging from approximately 760 to 4,500 μg g^{-1} Mo, and enrichment in light Mo isotopes with δ^{98}Mo spanning –0.3 ‰ to +0.2 ‰ (Table 1, Figure 4). They are also Fe-rich (11 to 42 wt. %, Table 1) and poorly crystalline, as indicated by a lack of Fe-(oxyhydr)oxide peaks in XRD, broad and diffuse selected-area electron diffractograms, and microscopic observations (Figures 6, S8, and S9). Ferrihydrite is present in samples SRD-S2, SRD-S4, and B-1A, as indicated by broad Raman bands around ~361, ~508, and ~707 cm^{-1} that are characteristic of that phase[61] (Figure 5). Minor amounts of other minerals are also present in some ochreous precipitate samples (Figures 5, S9, and S10). In particular, sample SRD-S1 has a unique phase assemblage that includes amorphous Fe-(oxyhydr)oxides, clays, quartz, feldspars, and minor hematite and algal detritus (Figures 5, 6, S8, and S9).

The association of Mo to Fe-(oxyhydr)oxides in SRD pond sediments was examined by XAS spectra obtained over the XANES and EXAFS regions. The XANES-LCF indicates that Mo in most samples is found as tetrahedral (*Td*) Mo(VI) bound to ferrihydrite by inner-sphere complexation (Figure 3). This bonding environment for Mo was corroborated through modelling of Mo K-edge EXAFS: the average Mo coordination number determined by EXAFS is ~ 4, with a first-shell neighboring O atom at an average distance of 1.76 to 1.77 Å (Table 2); the second-shell neighbor could be fitted as Fe in two types of coordination environments: (1) edge-sharing bidentate mononuclear bonding of Mo(VI) tetrahedra (Mo-Fe_1; in samples SRD-S2, SRD-S4, and B-1A) and (2) corner-sharing bidentate-binuclear bonding of Mo(VI) tetrahedra (Mo-Fe_2; in samples SRD-S2 and B-1A). No evidence of reduced Mo [*e.g.*, Mo(IV) or Mo(V)] was found (Figure S5).

The Mo coordination in SRD pond sample SRD-S1 is more complex, consistent with its more diverse phase assemblage (Figures 5, 6, S8, and S9). The XANES-LCF for this sample suggested a significant fraction (57 %) of Mo(VI) is present in octahedral coordination. The balance of its Mo was fitted as *Td* Mo(VI) sorbed to a combination of ferrihydrite, hematite, and amorphous $Al(OH)_{3(s)}$ (Figure 3). The presence of ferrihydrite and hematite in XANES-LCF is consistent with Raman and TEM analyses. Although $Al(OH)_{3(s)}$ was not identified in SRD-S1, this sample exhibited a relatively higher Al content and contained clay minerals (Figure S9). Clays can sorb Mo,[19,62,63] supporting the inclusion of a Mo-Al association in LCF. A reasonable EXAFS fit was obtained for SRD-S1 by a five-shell but heavily constrained model involving Mo-O, Mo-Al, and Mo-Fe interactions (Table 2).

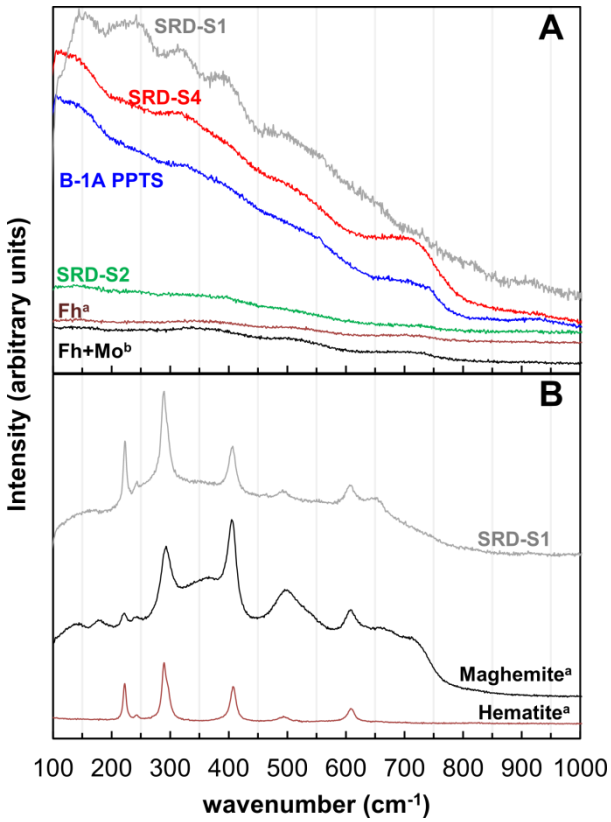

Figure 5. Select Raman spectra for ochreous precipitate samples. Panel A shows sample spectra compared to: ferrihydrite (Fh) and Mo adsorbed onto ferrihydrite from refs. [61,64] All samples have high fluorescence as a result of poor crystallinity. Samples SRD-S2, B-1A, and SRD-S4 have broad bands around 361, 508, and 707 cm^{-1} which correspond to poorly crystalline ferrihydrite. Panel B shows a spectrum from sample SRD-S1 that is consistent with the presence of hematite and/or maghemite.[61]

Table 1. Elemental abundances and Mo isotope ratios in ochreous precipitate samples

Sample ID	N-total	C-total	TIC	TOC	Na	Mn	Fe	Mg	Al	K	Ca	Mo	δ^{98}Mo	± *
	%	%	%	%	wt. %.	wt. %.	wt. %.	wt. %.	wt. %.	wt. %.	wt. %.	ppm	‰	
SRD-S1	0.33	2.9	0.40	2.5	0.98	1.2	11	0.41	4.2	1.5	0.36	760	-0.28	*0.02*
SRD-S2	0.13	1.8	0.77	1.0	0.25	0.77	38	0.030	0.31	<dl	0.43	4460	-0.02	*0.02*
SRD-S4	0.058	1.3	0.71	0.56	0.10	0.54	42	0.020	0.10	<dl	0.38	4390	0.24	*0.02*
SRD-W1 PPTS†	--	--	--	--	--	--	--	--	--	--	--	--	0.05	0.05
Mn-Buck†	--	--	--	--	--	--	--	--	--	--	--	--	-0.27	*0.02*
B-1A	--	--	--	--	0.13	1.0	36	0.040	0.070	0.060	0.60	840	-0.28	*0.01*

<dl indicates that the parameter was below detection limit, -- indicates that the parameter was not analyzed.

* Represents the two-standard-deviation of replicate δ^{98}Mo analyses on the MC-ICP-MS for samples analyzed more than once, or 2 SE for single analyses, denoted by italic font.

† For the samples SRD-W1 PPTS and Mn-Buck, elemental abundances could not be determined because the sample mass prior to digestion was not known.

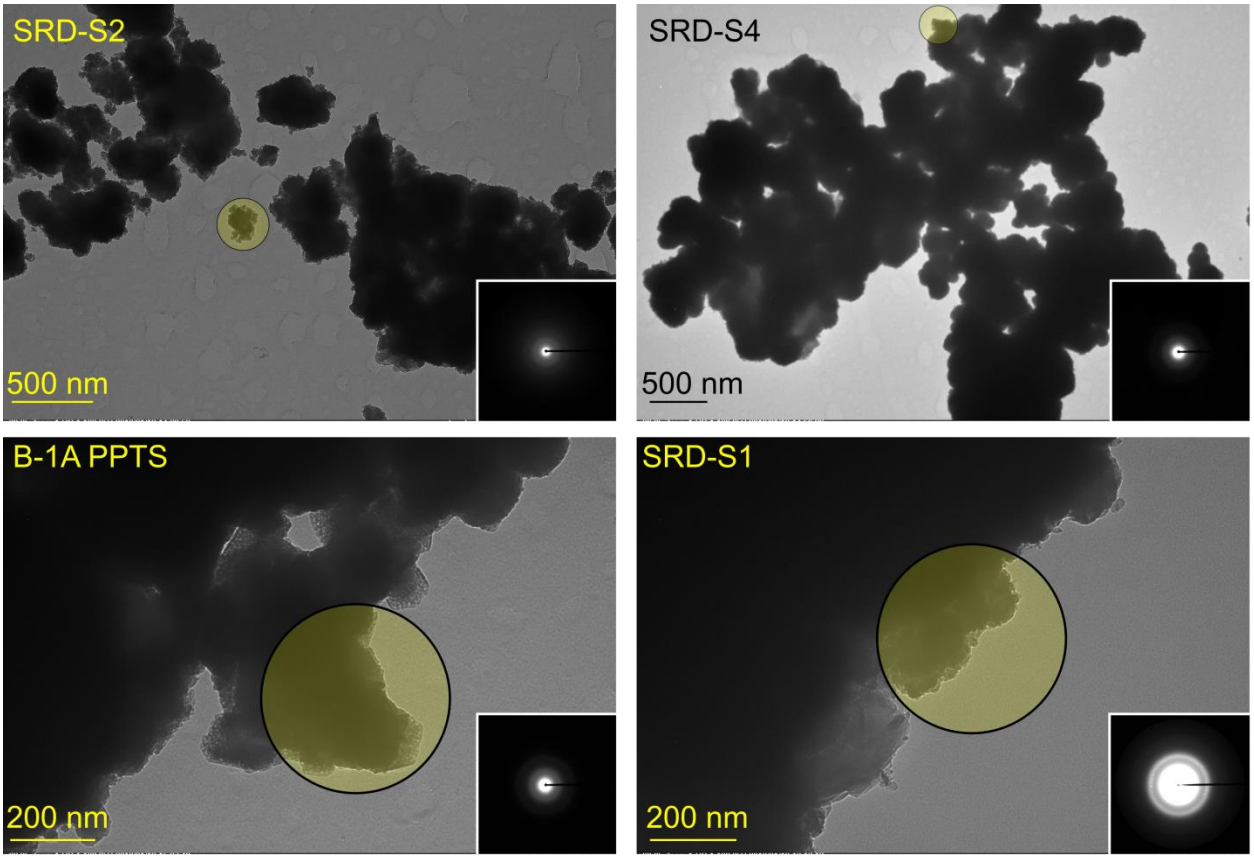

Figure 6. Selected transmission-electron microscopy images of Fe-(oxyhydr)oxide ochreous precipitates collected in the SRD. The approximate areas analyzed for electron diffraction and EDX are shown in yellow circles. Electron diffractograms are shown at bottom right; broad and diffuse rings indicate amorphous or nanocrystalline structure. Additional TEM images are shown in Figure S8.

3.2 Quantifying Mo isotope fractionation during attenuation

The isotope separation factor (Δ^{98}Mo) corresponding to sorption to ferrihydrite can be calculated by comparing δ^{98}Mo data of ochreous precipitates in the SRD pond and tailings sample with that of co-existing water samples:

$$\Delta^{98}Mo_{Fe\text{-}(oxyhydr)oxide\text{-}aqueous} = \delta^{98}Mo_{Fe(oxyhydr)oxide} - \delta^{98}Mo_{aqueous} \quad (2)$$

For ochreous precipitates, the apparent Δ^{98}Mo is –1.0 ± 0.4 ‰ (Table S2A; note that sample SRD-S1 was excluded from this calculation because of its mixed-phase assemblage). For tailings samples, a similar calculation can be done by isotopic mass balance with knowledge of δ^{98}Mo of the bulk sample, the relative Mo distribution between molybdenite and ferrihydrite from the XANES-LCF, and an estimate of δ^{98}Mo of TCM molybdenite (0.7 ‰; from ref.[11]). This calculation yields a similar Δ^{98}Mo of –1.2 ± 0.4 ‰ (Table S2B). The circa –1‰ isotope fractionation observed during Mo sorption on ferrihydrite matches the previously published value of –1.1 ± 0.2 ‰ determined from laboratory batch experiments.[21] The larger range in Δ^{98}Mo in our study probably reflects the greater sorption-site heterogeneity for environmental Fe-(oxyhydr)oxides in comparison to the synthetic ferrihydrite that was used in laboratory experiments.[21]

A Mo isotope fractionation factor can also be inferred from water samples along the flowpath from the tailings pond to the Rock Toe and SRD pond. A linearized Rayleigh model[59,60] gives an apparent Δ^{98}Mo of –0.7 ± 0.2 ‰ that provides a good fit to the data (Figure 2 and Figure S12). While this Δ^{98}Mo corroborates preferential removal of light Mo isotope following attenuation, it is smaller than the Δ^{98}Mo calculated directly from water-solid sample pairs above, which may be related to hydrodynamic dispersion, or due to co-occurrence of multiple Mo release and attenuation processes along the flowpath. Hydrodynamic dispersion typically decreases apparent

isotope fractionation under active-flow conditions.[65–68] In addition, the Rayleigh model assumes irreversible removal of reaction products;[60] however, anoxia in water-saturated tailings likely leads to reductive dissolution of Fe-(oxyhydr)oxides,[46] as evidenced by elevated dissolved Fe concentrations in Rock Toe seepage (Figure 1). Because Mo sorbed onto Fe-(oxyhydr)oxides is isotopically light,[11,21] reductive dissolution of these phases would release isotopically light Mo to tailings porewaters and decrease the magnitude of observed fractionation in tailings seepage. Apparent isotope fractionation on the anoxic portion of the flowpath (between the tailings pond and the Rock Toe) may also be influenced by processes other than Mo sorption onto Fe-(oxyhydr)oxides, including: (1) sorption onto pyrite and clays;[18,19] (2) precipitation of particle-reactive thiomolybdate (limited to sulfidic regions[26]); and (3) precipitation of powellite.[13] Pyrite and non-Fe(III) bearing clays (e.g., kaolinite) are expected to better withstand the reducing conditions in the TMF than Fe-(oxyhydr)oxides and are able to sorb Mo.[18,19] Conversion of molybdate to thiomolybdate, and its subsequent association to solid Fe(II)-sulfides can also sequester Mo in Fe- and sulfate-reducing settings,[26,69,70] although the substantial stoichiometric excess of Mo over dissolved sulfide at the Rock Toe suggests this process is of limited importance (Table S3). Else, Rock Toe seepage is consistently near powellite saturation (SI $\approx$ 0, Table S3 and Figure S7) and this phase has been identified as a Mo solubility control at other mine sites.[13,15,16] All of these reactions should preferentially remove light Mo isotopes from solution and could plausibly influence the apparent Δ^{98}Mo value derived from water-chemistry data in Figure 2.[21,38,39,56–58]

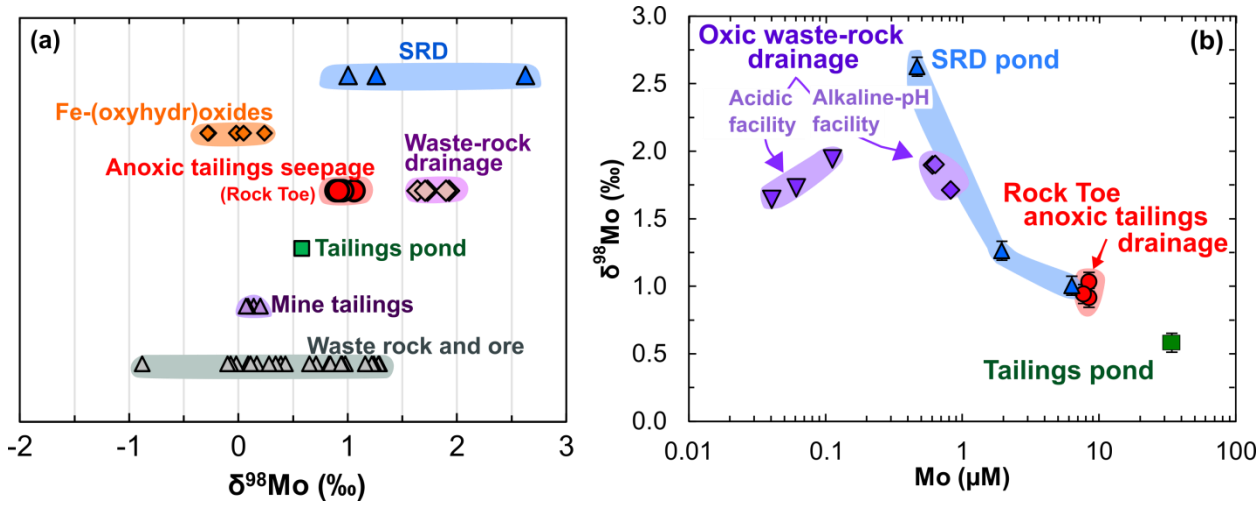

Figure 4. Left: comparison of δ^{98}Mo values in the SRD, Rock Toe, and Fe-(oxyhydr)oxides, shown along with TCM mine tailings, tailings pond, waste rock, and ore δ^{98}Mo from ref.[11] The ~0.4 ‰ increase in δ^{98}Mo between the tailings pond and the Rock Toe is attributed to minor Mo attenuation. Molybdenum sorption to Fe-(oxyhydr)oxides drives SRD pond waters towards even heavier δ^{98}Mo. Right: Anoxic tailings drainage at the Rock Toe has smaller Mo isotope fractionation and orders-of-magnitude higher [Mo] than that of oxic waste-rock drainage at the same site (data from ref.[11]), indicating greater Mo mobility in anoxic tailings environments.

Table 2. Summary of Mo K-edge EXAFS fitting parameters for ochreous precipitate samples.

	E_o (eV)	CN	R (Å)	σ^2 (Å^2)	R-Factor	χ_v^2
SRD-S4						
Mo–O	-4.1(9)	3.7(2)	1.764(4)	0.0036(5)	0.006	15.2
Mo–Fe$_1$		0.8(2)	2.79(2)	0.01*		
SRD-S2						
Mo–O	-5.0(8)	3.8(2)	1.763(3)	0.0041(4)	0.003	27.6
Mo–Fe$_1$		1.0(1)	2.79(1)	0.01*		
Mo–Fe$_2$		0.9(3)	3.56(2)	0.01*		
B-1A PPTS						
Mo–O	-3.6(9)	3.8(2)	1.770(4)	0.0047(5)	0.005	7.0
Mo–Fe$_1$		1.2(2)	2.80(1)	0.01*		
Mo–Fe$_2$		0.7(3)	3.54(3)	0.01[a]		
SRD-S1						
Mo–O$_{eq}$	-6(3)	3.3(2)	1.76(1)	0.006*	0.016	56
Mo–O$_{ax}$		1.3(3)	2.17(2)	0.006*		
Mo–Al		1*	2.50(4)	0.006*		
Mo–Fe$_1$		0.5*	2.65(3)	0.006*		
Mo–Fe$_2$		1*	3.29(2)	0.008*		

Fitting was performed over a range from k_{min} = 2.0 Å^{-1} to k_{max} = 11.0 Å^{-1}. The amplitude reduction factor, S_0^2, was fixed at 0.9. E_o = energy shift. R = interatomic distance. σ^2 = Debye-Waller factor. χ_v^2 = reduced chi square. The numbers in parentheses are the Artemis-provided errors calculated from the diagonal of the covariance matrix and scaled by the square-root of χ_v^2.

*Parameter held constant in the fitting procedure

3.3 Environmental implications

The consistent association of isotopically light Mo with Fe-(oxyhydr)oxides highlights the importance of sorption as an attenuation mechanism of Mo in oxic environments—a process which is traceable through Mo isotope analyses. This process is most evident during discharge and oxidation of Fe(II)-rich basal tailings seepage from the Rock Toe into the SRD pond (Figure S4). The water residence time in the SRD pond is estimated to be on the order of days, and yet there is an up to 18-fold decrease in Mo concentrations and 1.6 ‰ rise in δ^{98}Mo relative to input values (Rock Toe seepage) as a result of sorption of Mo onto Fe-(oxyhydr)oxide-rich sediment (Figure 1). In contrast, Mo concentrations decrease by a factor of approximately 4 and δ^{98}Mo increases by only 0.4 ‰ along the much longer and anoxic flowpath between the tailings pond and the Rock Toe, despite a considerably longer residence time (i.e., years). Consideration of Mo concentration and isotope data in waste-rock storage facilities at the same site further illustrates the importance of Mo sorption in oxic environments: waste-rock drainage is oxic and is characterized by Mo concentrations that are 1 to 2 orders of magnitude lower, and δ^{98}Mo that is 0.6 to 0.9 ‰ higher,[11] in comparison to the anoxic tailings seepage, (Figure 4). Given that δ^{98}Mo estimates of the Mo sources in these facilities is similar (0.6 for tailings pond seepage and 0.7 ‰ for TCM molybdenite)[9] and that δ^{98}Mo rises values following attenuation,[21,22,25,38–40,56–58,71] it follows that Mo mobility is greater in anoxic tailings seepage than in oxic waste-rock drainage where greater Mo isotope fractionation is observed. This difference is likely related to decreased availability of Fe-(oxyhydr)oxides in the anoxic TMF due to their instability under reducing conditions; in contrast Fe-(oxyhydr)oxides are widespread in oxic waste-rock storage facilities that contain pyrite and which are generally water-unsaturated (due to coarser particle size) and thus better oxygenated.[45] A broad review of Mo occurrence in natural waters has also identified anoxic and

Fe-reducing (but with low dissolved sulfide) conditions as having potential for enhanced Mo mobilization[3], i.e., analogous geochemical conditions to the anoxic tailing seepage studied here [note that under anoxic and high dissolved sulfide conditions, Mo can co-precipitate with Fe(II) and S].[70,72]

The stability of inner-sphere Mo complexes sorbed on Fe-(oxyhydr)oxides has implications for long-term water-quality in mine wastes, and is tied to aqueous geochemical conditions. In particular, dissolution and/or phase transformation of Fe-(oxyhydr)oxides can occur under anoxic or strongly acidic (pH < about 3.5) conditions, which may remobilize sorbed Mo.[43,44,73] However, such Mo remobilization is likely to be traceable through Mo isotope analyses given the enrichment of isotopically light Mo on sorption surfaces.

Molybdenum contamination in groundwater is not necessarily limited to mining environments,[74] making Mo isotopes a useful tracer of Mo transport and attenuation in a variety of settings. In the most general sense, a lack of Mo isotope fractionation in water relative to source minerals reflects direct mineral dissolution, while rising δ^{98}Mo indicates attenuation. Sorption of Mo onto oxides and (oxyhydr)oxides is likely to be the dominant process driving Mo attenuation and isotope fractionation under most oxic environments, with the exception of specific settings enriched in Mo at high enough levels to induce precipitation of molybdate minerals (*e.g.*, Mo ore deposits). Sorption also generates the largest Mo isotope fractionation factors (see a recent compilation in ref.[11]). While alternate Mo attenuation mechanisms may also be available under anoxic conditions (*e.g.*, molybdate and thiomolybdate phase precipitation, and Mo sorption onto clays and/or pyrite), they appeared to have limited effect at decreasing Mo solubility and causing Mo isotope fractionation in the tailings seepage studied here.

Acknowledgements

This study was financed through a Natural Science and Engineering Research Council (NSERC) Canada Graduate Scholarship to EKS and the MAGNET (NSERC-CREATE) program. Additional financial support was provided by Lorax Environmental. We are grateful to TCM staff, in particular Bert Doughty, Chris Natoli, Ray Cheff, and Richard Giampedraglia, for providing site access. Dr. Gregor Lucic and Laura Laurenzi also assisted with fieldwork. Dr. Marghaleray Amini, Kathy Gordon, Maureen Soon, Dr. Elisabetta Pani, Jenny Lai, and Lan Kato are thanked for assistance in the operation of analytical instrumentation at UBC. XAS analyses were conducted at the HXMA beamline (06ID-1) at the Canadian Light Source (CLS), which is supported by the Canada Foundation for Innovation, NSERC, the University of Saskatchewan, the Government of Saskatchewan, Western Economic Diversification Canada, the National Research Council Canada, and the Canadian Institutes of Health Research. Drs. Ning Chen and Weifeng Chen are thanked for their assistance at the CLS. We thank Dr. Shaun Brown and two anonymous reviewers for their constructive reviews.

4 References

(1) Kaback, D. S.; Runnells, D. D. Geochemistry in some stream sediments and waters. *Geochim. Cosmochim. Acta* **1980**, *44*, 447–456.

(2) Goumih, A.; El Adnani, M.; Hakkou, R.; Benzaazoua, M. Geochemical Behavior of Mine Tailings and Waste Rock at the Abandoned Cu–Mo–W Azegour Mine (Occidental High Atlas, Morocco). *Mine Water Environ.* **2013**, *32*, 121–132.

(3) Smedley, P. L.; Kinniburgh, D. G. Molybdenum in natural waters: A review of occurrence, distributions and controls. *Appl. Geochemistry* **2017**, *84*, 387–432.

(4) Solongo, T.; Fukushi, K.; Altansukh, O.; Takahashi, Y.; Akehi, A.; Baasansuren, G.; Ariuntungalag, Y.; Enkhjin, O.; Davaajargal, B.; Davaadorj, D.; Hasebe, N. Distribution and Chemical Speciation of Molybdenum in River and Pond Sediments Affected by Mining Activity in Erdenet City, Mongolia. *Minerals* **2018**, *8*, 288.

(5) Erdman, J. A.; Ebens, R. J.; Case, A. A. Molybdenosis: A Potential Problem in Ruminants Grazing on Coal Mine Spoils. *J. Range Manag.* **1978**, *31*, 34.

(6) World Health Organization. *Molybdenum in Drinking-water*, *Background document for development of WHO Guidelines for Drinking-Water Quality*; 2011.

(7) Skierszkan, E. K.; Mayer, K. U.; Weis, D.; Beckie, R. D. Molybdenum and zinc stable isotope variation in mining waste rock drainage and waste rock at the Antamina mine, Peru. *Sci. Total Environ.* **2016**, *550*, 103–113.

(8) Frascoli, F.; Hudson-Edwards, K. Geochemistry, Mineralogy and Microbiology of Molybdenum in Mining-Affected Environments. *Minerals* **2018**, *8*, 42.

(9) Skierszkan, E. K.; Mayer, K. U.; Weis, D.; Beckie, R. D. Molybdenum and zinc stable isotope variation in mining waste rock drainage and waste rock at the Antamina mine , Peru. *Sci. Total Environ.* **2016**, *550*, 103–113.

(10) Essilfie-Dughan, J.; Hendry, M. J.; Pickering, I. J.; George, G.; Kotzer, T. Molybdenum and selenium speciation in uranium mine tailings using X-ray absorption spectroscopy. *Environ. Sci. Technol.* **2011**, *45*, 455–460.

(11) Skierszkan, E. K.; Stockwell, J. S.; Dockrey, J. W.; Weis, D.; Beckie, R. D.; Mayer, K. U.

Molybdenum (Mo) stable isotopic variations as indicators of Mo attenuation in mine waste-rock drainage. *Appl. Geochemistry* **2017**, *87*, 71–83.

(12) Hirsche, D. T.; Blaskovich, R.; Mayer, K. U.; Beckie, R. D. A study of Zn and Mo attenuation by waste-rock mixing in neutral mine drainage using mixed-material field barrels and humidity cells. *Appl. Geochemistry* **2017**, *84*, 114–125.

(13) Conlan, M. J. W.; Mayer, K. U.; Blaskovich, R.; Beckie, R. D. Solubility controls for molybdenum in neutral rock drainage. *Geochemistry Explor. Environ. Anal.* **2012**, *12*, 21–32.

(14) Langedal, M. Dispersion of tailings in the Knabeåna-Kvina drainage basin, Norway, 2: Mobility of Cu and Mo in tailings-derived fluvial sediments. *J. Geochemical Explor.* **1997**, *58*, 173–183.

(15) Blanchard, P. E. R.; Hayes, J. R.; Grosvenor, A. P.; Rowson, J.; Hughes, K.; Brown, C. Investigating the geochemical model for molybdenum mineralization in the JEB tailings management facility at McClean Lake, Saskatchewan: An x-ray absorption spectroscopy study. *Environ. Sci. Technol.* **2015**, *49*, 6504–6509.

(16) Hayes, J. R.; Grosvenor, A. P.; Rowson, J.; Hughes, K.; Frey, R. A.; Reid, J. Analysis of the Mo speciation in the JEB tailings management facility at McClean Lake, Saskatchewan. *Environ. Sci. Technol.* **2014**, *48*, 4460–4467.

(17) Bissonnette, J.; Essilfie-Dughan, J.; Moldovan, B. J.; Hendry, M. J. Sequestration of As and Mo in uranium mill precipitates (pH 1.5–9.2): An XAS study. *Appl. Geochemistry* **2016**, *72*, 30–33.

(18) Bostick, B. C.; Fendorf, S. S.; Helz, G. R. Differential Adsorption of Molybdate and Tetrathiomolybdate on Pyrite. *Environ. Sci. Technol.* **2003**, *37*, 285–291.

(19) Goldberg, S.; Forster, H. S.; Godfrey, C. L. Molybdenum Adsorption on Oxides, Clay Minerals, and Soils. *Soil Sci. Soc. Am. J.* **1996**, *60*, 425.

(20) Gustafsson, J. P.; Tiberg, C. Molybdenum binding to soil constituents in acid soils: An XAS and modelling study. *Chem. Geol.* **2015**, *417*, 279–288.

(21) Goldberg, T.; Archer, C.; Vance, D.; Poulton, S. W. Mo isotope fractionation during

adsorption to Fe (oxyhydr)oxides. *Geochim. Cosmochim. Acta* **2009**, *73*, 6502–6516.

(22) Kashiwabara, T.; Takahashi, Y.; Tanimizu, M.; Usui, A. Molecular-scale mechanisms of distribution and isotopic fractionation of molybdenum between seawater and ferromanganese oxides. *Geochim. Cosmochim. Acta* **2011**, *75*, 5762–5784.

(23) Arai, Y. X-ray absorption spectroscopic investigation of molybdenum multinuclear sorption mechanism at the goethite-water interface. *Environ. Sci. Technol.* **2010**, *44*, 8491–8496.

(24) Goldberg, S.; Forster, H. S. Factors affecting molybdenum adsorption by soils and minerals. *Soil Sci.* **1998**, *163*, 109–114.

(25) Skierszkan, E. K.; Mayer, K. U.; Weis, D.; Robertson, J.; Beckie, R. D. Molybdenum stable isotope fractionation during the precipitation of powellite (CaMoO4) and wulfenite (PbMoO4). *Geochim. Cosmochim. Acta* **2019**, *244*, 383–402.

(26) Helz, G. R.; Miller, C. V.; Charnock, J. M.; Mosselmans, J. F. W.; Pattrick, R. A. D.; Garner, C. D.; Vaughan, D. J. Mechanism of molybdenum removal from the sea and its concentration in black shales: EXAFS evidence. *Geochim. Cosmochim. Acta* **1996**, *60*, 3631–3642.

(27) Wiederhold, J. G. Metal stable isotope signatures as tracers in environmental geochemistry. *Environ. Sci. Technol.* **2015**, *49*, 2606–2624.

(28) Ellis, A. S.; Johnson, T. M.; Bullen, T. D. Cr isotopes ratios and the fate of hexavalent chromium in the environment. *Science (80-.).* **2002**, *295*, 2060–2062 [12–6].

(29) Jamieson-Hanes, J. H.; Gibson, B. D.; Lindsay, M. B. J.; Kim, Y.; Ptacek, C. J.; Blowes, D. W. Chromium isotope fractionation during reduction of Cr(VI) under saturated flow conditions. *Environ. Sci. Technol.* **2012**, *46*, 6783–6789.

(30) Basu, A.; Brown, S. T.; Christensen, J. N.; Depaolo, D. J.; Reimus, P. W.; Heikoop, J. M.; Woldegabriel, G.; Simmons, A. M.; House, B. M.; Hartmann, M.; Maher, K. Isotopic and geochemical tracers for U(VI) reduction and U mobility at an in situ recovery U mine. *Environ. Sci. Technol.* **2015**, *49*, 5939–5947.

(31) Jemison, N. E.; Shiel, A. E.; Johnson, T. M.; Lundstrom, C. C.; Long, P. E.; Williams, K. H. Field Application of 238U/235U Measurements to Detect Reoxidation and Mobilization

of U(IV). *Environ. Sci. Technol.* **2018**, *52*, 3422–3430.

(32) Jemison, N. E.; Johnson, T. M.; Shiel, A. E.; Lundstrom, C. C. Uranium isotopic fractionation induced by U(VI) adsorption onto common aquifer minerals. *Environ. Sci. Technol.* **2016**, *50*, 12232–12240.

(33) Shiel, A. E.; Laubach, P. G.; Johnson, T. M.; Lundstrom, C. C.; Long, P. E.; Williams, K. H. No measurable changes in 238U/235U due to desorption-adsorption of U(VI) from groundwater at the Rifle, Colorado, integrated field research challenge site. *Environ. Sci. Technol.* **2013**, *47*, 2535–2541.

(34) Shrimpton, H. K.; Blowes, D. W.; Ptacek, C. J. Fractionation of Selenium during Selenate Reduction by Granular Zerovalent Iron. *Environ. Sci. Technol.* **2015**, *49*, 11688–11696.

(35) Veeramani, H.; Eagling, J.; Jamieson-Hanes, J. H.; Kong, L.; Ptacek, C. J.; Blowes, D. W. Zinc isotope fractionation as an indicator of geochemical attenuation processes. *Environ. Sci. Technol. Lett.* **2015**, *2*, 314–319.

(36) Lane, S.; Proemse, B. C.; Tennant, A.; Wieser, M. E. Concentration measurements and isotopic composition of airborne molybdenum collected in an urban environment. *Anal. Bioanal. Chem.* **2013**, *405*, 2957–2963.

(37) Kendall, B.; Dahl, T. W.; Anbar, A. D. the Stable Isotope Geochemistry of Molybdenum. *Rev. Mineral. Geochemistry* **2017**, *82*, 683–732.

(38) Wasylenki, L. E.; Weeks, C. L.; Bargar, J. R.; Spiro, T. G.; Hein, J. R.; Anbar, A. D. The molecular mechanism of Mo isotope fractionation during adsorption to birnessite. *Geochim. Cosmochim. Acta* **2011**, *75*, 5019–5031.

(39) Kashiwabara, T.; Kubo, S.; Tanaka, M.; Senda, R.; Iizuka, T.; Tanimizu, M.; Takahashi, Y. Stable isotope fractionation of tungsten during adsorption on Fe and Mn (oxyhydr)oxides. *Geochim. Cosmochim. Acta* **2017**, *204*, 52–67.

(40) Kashiwabara, T.; Takahashi, Y.; Tanimizu, M. A XAFS study on the mechanism of isotopic fractionation of molybdenum during its adsorption on ferromanganese oxides. *Geochem. J.* **2009**, *43*, 31–36.

(41) Nägler, T. F.; Anbar, A. D.; Archer, C.; Goldberg, T.; Gordon, G. W.; Greber, N. D.;

Siebert, C.; Sohrin, Y.; Vance, D. Proposal for an International Molybdenum Isotope Measurement Standard and Data Representation. *Geostand. Geoanalytical Res.* **2014**, *38*, 149–151.

(42) Lindsay, M. B. J.; Moncur, M. C.; Bain, J. G.; Jambor, J. L.; Ptacek, C. J.; Blowes, D. W. Geochemical and mineralogical aspects of sulfide mine tailings. *Appl. Geochemistry* **2015**, *57*, 157–177.

(43) Blowes, D. W.; Ptacek, C. J.; Jambor, J. L.; Weisener, C. G.; Paktunc, D.; Gould, W. D.; Johnson, D. B. *The Geochemistry of Acid Mine Drainage*; 2nd ed.; Elsevier Ltd., 2014; Vol. 11.

(44) Qin, K. Impact of iron(II)-induced transformation of iron(III) hydr(oxides) on molybdenum mobility in groundwater. MSc Thesis., University of Saskatchewan, 2016.

(45) Lorca, M. E.; Mayer, K. U.; Pedretti, D.; Smith, L.; Beckie, R. D. Spatial and Temporal Fluctuations of Pore-Gas Composition in Sulfidic Mine Waste Rock. *Vadose Zo. J.* **2016**, *15*, 0.

(46) Lorax Environmental Services Ltd. *Thompson Creek Mine Tailings Impoundment – Geochemical Characterization and Water Quality Predictions. Lorax Environmental Services Ltd., Vancouver BC*; 2011.

(47) Edmond, J. M. High precision determination of titration alkalinity and total carbon dioxide content of seawater by potentiometric titration. *Deep. Res.* **1970**, *17*, 737–750.

(48) Axelsson, M. D.; Rodushkin, I.; Ingri, J.; Öhlander, B. Multielemental analysis of Mn-Fe nodules by ICP-MS: Optimisation of analytical method. *Analyst* **2002**, *127*, 76–82.

(49) Connelly, J. N.; Ulfbeck, D. G.; Thrane, K.; Bizzarro, M.; Housh, T. A method for purifying Lu and Hf for analyses by MC-ICP-MS using TODGA resin. *Chem. Geol.* **2006**, *233*, 126–136.

(50) Skierszkan, E. K.; Amini, M.; Weis, D. A practical guide for the design and implementation of the double-spike technique for precise determination of molybdenum isotope compositions of environmental samples. *Anal. Bioanal. Chem.* **2015**, *407*, 1925–1935.

(51) Migeon, V.; Bourdon, B.; Pili, E.; Fitoussi, C. Molybdenum isotope fractionation during

acid leaching of a granitic uranium ore. *Geochim. Cosmochim. Acta* **2018**, *231*, 30–49.

(52) Siebert, C.; Nägler, T. F.; von Blanckenburg, F.; Kramers, J. D. Molybdenum isotope records as a potential new proxy for paleoceanography. *Earth Planet. Sci. Lett.* **2003**, *211*, 159–171.

(53) Pearce, C. R.; Burton, K. W.; von Strandmann, P. A. E. P.; James, R. H.; Gíslason, S. R. Molybdenum isotope behaviour accompanying weathering and riverine transport in a basaltic terrain. *Earth Planet. Sci. Lett.* **2010**, *295*, 104–114.

(54) Voegelin, A. R.; Nägler, T. F.; Pettke, T.; Neubert, N.; Steinmann, M.; Pourret, O.; Villa, I. M. The impact of igneous bedrock weathering on the Mo isotopic composition of stream waters: Natural samples and laboratory experiments. *Geochim. Cosmochim. Acta* **2012**, *86*, 150–165.

(55) Siebert, C.; Pett-Ridge, J. C.; Opfergelt, S.; Guicharnaud, R. A.; Halliday, A. N.; Burton, K. W. Molybdenum isotope fractionation in soils: Influence of redox conditions, organic matter, and atmospheric inputs. *Geochim. Cosmochim. Acta* **2015**, *162*, 1–24.

(56) Barling, J.; Anbar, A. D. Molybdenum isotope fractionation during adsorption by manganese oxides. *Earth Planet. Sci. Lett.* **2004**, *217*, 315–329.

(57) Wasylenki, L. E.; Rolfe, B. A.; Weeks, C. L.; Spiro, T. G.; Anbar, A. D. Experimental investigation of the effects of temperature and ionic strength on Mo isotope fractionation during adsorption to manganese oxides. *Geochim. Cosmochim. Acta* **2008**, *72*, 5997–6005.

(58) King, E. K.; Perakis, S. S.; Pett-Ridge, J. C. Molybdenum isotope fractionation during adsorption to organic matter. *Geochim. Cosmochim. Acta* **2018**, *222*, 584–598.

(59) Scott, K. M.; Lu, X.; Cavanaugh, C. M.; Liu, J. S. Optimal methods for estimating kinetic isotope effects from different forms of the Rayleigh distillation equation. *Geochim. Cosmochim. Acta* **2004**, *68*, 433–442.

(60) Rayleigh, Lord. On the distillation of binary mixtures. *London, Edinburgh, Dublin Philos. Mag. J. Sci.* **1902**, *4*, 521–537.

(61) Das, S.; Hendry, M. J. Application of Raman spectroscopy to identify iron minerals commonly found in mine wastes. *Chem. Geol.* **2011**, *290*, 101–108.

(62) Sun, W.; Selim, H. M. Kinetics of Molybdenum Adsorption and Desorption in Soils. *J. Environ. Qual.* **2018**, *47*, 504–512.

(63) Goldberg, S.; Su, C.; Forster, H. S. Sorption of Molybdenum on Oxides, Clay Minerals, and Soils: Mechanisms and Models. In *Adsorption of Metals by Geomedia*; 1998; pp. 401–426.

(64) Das, S.; Essilfie-Dughan, J.; Jim Hendry, M. Sequestration of molybdate during transformation of 2-line ferrihydrite under alkaline conditions. *Appl. Geochemistry* **2016**, *73*, 70–80.

(65) Jamieson-Hanes, J. H.; Amos, R. T.; Blowes, D. W. Reactive transport modeling of chromium isotope fractionation during Cr(VI) reduction. *Environ. Sci. Technol.* **2012**, *46*, 13311–13316.

(66) Abe, Y.; Hunkeler, D. Does the Rayleigh equation apply to evaluate field isotope data in contaminant hydrogeology? *Environ. Sci. Technol.* **2006**, *40*, 1588–1596.

(67) Druhan, J. L.; Maher, K. The influence of mixing on stable isotope ratios in porous media: A revised Rayleigh Model. *Water Resour. Res.* **2017**, *53*, 1101–1124.

(68) Van Breukelen, B. M.; Prommer, H. Beyond the rayleigh equation: Reactive transport modeling of isotope fractionation effects to improve quantification of biodegradation. *Environ. Sci. Technol.* **2008**, *42*, 2457–2463.

(69) Erickson, B. E.; Helz, G. R. Molybdenum(VI) speciation in sulfidic waters: Stability and lability of thiomolybdates. *Geochim. Cosmochim. Acta* **2000**, *64*, 1149–1158.

(70) Dahl, T. W.; Chappaz, A.; Fitts, J. P.; Lyons, T. W. Molybdenum reduction in a sulfidic lake: Evidence from X-ray absorption fine-structure spectroscopy and implications for the Mo paleoproxy. *Geochim. Cosmochim. Acta* **2013**, *103*, 213–231.

(71) Nägler, T. F.; Neubert, N.; Böttcher, M. E.; Dellwig, O.; Schnetger, B. Molybdenum isotope fractionation in pelagic euxinia: Evidence from the modern Black and Baltic Seas. *Chem. Geol.* **2011**, *289*, 1–11.

(72) Helz, G. R.; Bura-Nakić, E.; Mikac, N.; Ciglenečki, I. New model for molybdenum behavior in euxinic waters. *Chem. Geol.* **2011**, *284*, 323–332.

(73) Cornell, R. M.; Schwertmann, H. C. U. *The Iron Oxides: Structure, Properties, Reactions,*

Occurences and Uses; 1st ed.; Wiley-VCH Verlag GmbH & Co. KGaA: Weinheim, Germany, 2003.

(74) Pichler, T.; Mozaffari, A. Distribution and mobility of geogenic molybdenum and arsenic in a limestone aquifer matrix. *Appl. Geochemistry* **2015**, *63*, 623–633.